ELSEVIER

Biophysical Chemistry 93 (2001) 197–213

Biophysical Chemistry

www.elsevier.com/locate/bpc

Boundary element modeling of biomolecular transport ☆

Stuart A. Allison

Department of Chemistry, Georgia State University, Atlanta, GA 30303, USA

Received 11 May 2001; received in revised form 10 May 2001; accepted 11 May 2001

Abstract

The boundary element (BE) methodology has emerged as a powerful tool in modeling a broad range of different transport phenomena of biomolecules in dilute solution. These include: sedimentation, diffusion (translational and rotational), intrinsic viscosity, and free solution electrophoresis. Modeling is carried out in the framework of the continuum primitive model where the biomolecule is modeled as an arbitrary array of solid platelets that contains fixed charges within. The surrounding fluid is modeled as a electrodynamic/hydrodynamic continuum which obeys the Poisson and low Reynolds number Navier–Stokes equations. Ion relaxation (the distortion of the ion atmosphere from equilibrium) can also be accounted for by solving the coupled ion transport equation (for each mobile ion species present), Poisson, and Navier–Stokes equations in tandem. Several examples are presented in this work. It is first applied to a detailed model of 20 bp DNA and it is concluded that it is not necessary to include a layer of bound water to reconcile experimental and model translational diffusion constants. With regards to diffusion, the BE approach is also applied to a 375-bp supercoiled DNA model (without ion relaxation), and also 20–60-bp DNA fragments with ion relaxation included in order to assess the magnitude of the electrolyte friction effect under a number of different salt/buffer conditions. Attention is then turned to modeling the electrophoretic mobility of three different cases. First of all, we consider a sphere with a central charge large enough in magnitude to insure that ion relaxation is significant. Excellent agreement with independent theory is obtained. Finally, it is applied to modeling short DNA fragments in KCl and Tris acetate salts. Quantitative agreement is achieved when the salt is KCl, but the calculated (absolute) mobility in Tris acetate is substantially higher than the experimental value. The interpretation of this is that there is an association between $Tris^+$ and DNA (perhaps hydrogen bonding) not accounted for in our modeling that is responsible for this discrepancy.

Keywords: Boundary element (BE); Transport phenomena; Biomolecules

☆ This work is based on a talk given at the 1-day Discussion Meeting of the British Biophysical Society entitled 'The Solvation/Hydration Problem in Solution Biophysics' at the University of Glasgow (Scotland) on 12 September 2000.

E-mail address: chesaa@panther.gsu.edu (S.A. Allison).

0301-4622/01/$ - see front matter
PII: S0301-4622(01)00221-6

1. Introduction

Sedimentation, translational, and rotational diffusion constants as well as intrinsic viscosities are transport properties that provide useful information about the size and possibly shape of biomolecules or particles in dilute aqueous solution. These transport properties are measurable by a variety of experimental techniques including ultracentrifugation [1] (sedimentation), polarized and depolarized dynamic light scattering [2–4] (translational and rotational diffusion constants), fluorescence depolarization [5,6] (rotational diffusion constants), NMR [4,6], and various viscometric methods [7] (intrinsic viscosity). In order to interpret these transport properties, it is usual to assume that the fluid surrounding the particle can be treated as a hydrodynamic continuum with uniform viscosity η (Newtonian fluid). It is convenient to define a solvent accessible surface, S_{sas}, that is generated by 'rolling' a probe sphere of radius σ_d over a space filling model of the biomolecule or particle [8]. For water, $\sigma_d = 1.4$ Å is appropriate since this corresponds to the distance of closest approach of the oxygen atoms in water [9]. Moving outward from S_{sas} into the fluid, the local viscosity changes from a high value to η over a narrow region. An additional assumption usually made is to contract this narrow region to a smooth surface enveloping the particle called the hydrodynamic shear surface, S_{hyd}. Experiments on a number of systems have shown that S_{hyd} is located at 1 ± 1 Å from the actual particle–solution interface, or S_{sas} [10]. Traditionally, inferences about particle size and shape have been made by interpreting transport properties in terms of simple geometrical models such as axisymmetric ellipsoids, long rods, and random coils [11,12]. Over the last 25 years, it has become possible to interpret these transport properties in terms of detailed, possibly atomic resolution models. The development of these modeling techniques is particularly timely given the current availability and sheer volume of high resolution structural information. Basically, two distinct but related modeling techniques have emerged. In the 'bead method' approach, which has its roots in the pioneering work of Kirkwood and coworkers [13] and subsequent investigators [14], the particle is modeled as an array of beads which can, in the general case, be of unequal size and overlapping. The literature on the bead method approach is extensive and only a few articles shall be cited here [15–19]. In the boundary element (BE) approach, the particle is represented as a closed, but arbitrary rigid body made up of a series of interconnected platelets and the assumption is made that various physical quantities (hydrodynamic stress forces, for example) are uniform over individual platelets, but can vary from one platelet to another. The application of the BE approach to purely hydrodynamic transport is also extensive [20–24]. In a formal sense, the 'bead' and BE approaches are closely related with the fundamental hydrodynamic units being spheres in the former case and platelets in the latter case. Both allow detailed modeling of the hydrodynamic shear surface, S_{hyd} and a comparison of that surface with the solvent accessible surface, S_{sas}. This, in turn, allows us to investigate whether or not there exists a layer of water which moves with the particle as a rigid object, and that is a question of considerable interest in this special issue of *Biophysical Chemistry*.

In addition to the transport properties mentioned in the previous paragraph, which provide size/shape information about biomolecules and particles, there are additional transport properties measured in the presence of electric fields that provide information about biomolecular charge as well. Perhaps the most notable of these transport properties is the electrophoretic mobility. The various electrophoretic methods [25] have proven to be of enormous value as a separation technique, but have not been widely used as structural probes because the complex interaction between macroion, solvent, mobile salt, gel (if present), and external electric field has made it difficult to interpret electrophoretic mobilities. In the absence of a gel support medium, which is called 'free solution' electrophoresis, the problem of interpretation is more straightforward and recent developments in membrane confined analytical electrophoresis [26], and capillary electrophoresis [27] have made free solution electrophoresis a viable experimental method for

comparatively large and highly charged biomolecules. The underlying model used in classical electrophoresis theory is similar to the continuum hydrodynamic model discussed in the preceding paragraph, but account must also be taken of the particle charge, its distribution, and the ion atmosphere. Additional model assumptions include: the polyion interior and solvent are modeled by uniform dielectric constants ε_i and ε_o, respectively; the mobile ions are modeled as a continuum and their distribution around the polyion satisfies the Poisson equation [28]; and the transport of each mobile ion present obeys an ion transport equation. For a charged particle undergoing steady state motion in a constant electric and/or flow field, it is also necessary to account for the distortion of the ion atmosphere from its equilibrium value. This 'ion relaxation' effect will be important unless the polyion is weakly charged [29,30]. What makes this a substantially more difficult problem than the transport of a uncharged particle is that the fluid motion (via the low Reynolds number Navier–Stokes equation) becomes inextricably coupled with the Poisson and ion transport equations. Until recently, this classical theory had only been applied to simple model structures such as spheres with a centrosymmetric charge distribution [29,31–33], long cylinders [34,35], or non-uniformly charged spheres with 'thin double layers' [36]. However, it is possible to solve the problem for polyions of arbitrary shape and charge distribution by an iterative BE procedure [37–39].

In general, charge effects influence sedimentation and diffusion constants as well as intrinsic viscosities even when external electric fields are not present. The best way to understand this is to consider the example of a sedimenting, highly charged polyion such as a DNA fragment. The streaming flow of solvent past the fragment will distort the ion atmosphere and give rise to an additional viscous drag, or 'electrolyte friction' [40–46] not present for the corresponding uncharged fragment, and this reduces sedimentation and diffusion constants. Similarly, 'ion relaxation' increases the intrinsic viscosity of a dilute suspension or rigid polyions placed in a fluid shear field, and this phenomenon is referred to as the 'primary electroviscous effect' [47–50]. For a review of these issues, the reader is referred to the text by Schmitz [51]. The effects of charge on sedimentation and diffusion are expected to be small and perhaps negligible for a weakly charged biomolecule in high salt, but the effect becomes more important as the polyion charge increases or the ambient salt concentration decreases. For a highly charged polyion such as DNA at low salt, we feel it is worth considering the effects of charge on sedimentation and diffusion.

The overall objective of the present work is to demonstrate the power and versatility of BE modeling as applied to an array of transport phenomena in use in biophysics today. The hydrodynamic BE approach is first reviewed and it is then applied to a number of problems. First, detailed models of short DNA fragments are examined in the absence of ion relaxation and the diffusion constants compared to experiment. The same approach is then applied to a wormlike chain-cylinder model of a 375-bp supercoiled DNA to illustrate the application of BE modeling to large and complex biomolecules. Next, we review how 'ion relaxation' is accounted for in the BE procedure and this more general algorithm is then used to determine the translational diffusion constants of the same short DNA model fragments considered previously in order to gauge the significance of electrolyte friction at several salt concentrations. The application of the BE procedure to determine free solution steady state electrophoretic mobilities of model polyions is discussed next. To test the modeling procedure with regards to the electrophoretic mobility, it is first applied to a sphere: (a) sufficiently charged to insure that ion relaxation substantially reduces the mobility; and (b) under conditions that make direct comparison with independent theory possible. The mobility of 20-bp DNA models is then considered and the effects of the ion atmosphere, surface model, and ion relaxation examined. At 11 M KCl, the calculated and experimental mobilities are compared and shown to be in excellent agreement with each other. Finally, we briefly consider buffer effects on the mobility of short DNA fragments to illus-

trate how the modeling procedures employed in this work may be of use in studying the 'binding' of ions to biomolecules.

2. Boundary element methodology

The boundary element (BE) method has been thoroughly discussed in previous work [20–24,37–39,50] so the present treatment shall be kept primarily to the form of an outline. The hydrodynamic portion of BE modeling will be presented in more depth in order to illustrate the approach to the reader who may have some familiarity with hydrodynamics, but not the BE methodology. The texts by Ladyzhenskaya [52] and Kim and Karrila [22] are excellent sources of information on hydrodynamic theory from the BE perspective.

The particle is assumed to be a rigid body with hydrodynamic shear surface, S_{hyd}, entirely enclosing it. On S_{hyd}, the assumption is made that the particle velocity and local fluid velocity are equal and this is called the 'stick' hydrodynamic boundary condition. An alternative boundary condition, called 'slip', corresponds to matching only the normal component of the particle and fluid velocities on S_{hyd} along with the additional assumption that there is no tangential component of stress on S_{hyd} [53]. Although there are cases which appear to be better described by the 'slip' rather than 'stick' boundary condition, such as the rotational diffusion of simple aromatic molecules in non-aqueous solvents [54], there is general agreement that the 'stick' case is appropriate for biomolecules in aqueous solvent. Although it is possible to apply BE modeling to the 'slip' case [21,24,53], the present work shall be limited to the 'stick' boundary condition. The solvent is represented as a Newtonian fluid with viscosity and the assumption is made that the motion of the particle is small enough so that the local fluid velocity, $\boldsymbol{v}$, and pressure, p, are well described by the linearized Navier–Stokes and solvent incompressibility equations

$$\eta\nabla^2\boldsymbol{v}(\boldsymbol{y}) - \boldsymbol{\nabla}p(\boldsymbol{y}) = -\boldsymbol{s}(\boldsymbol{y}) \tag{1}$$

$$\boldsymbol{\nabla}\cdot\boldsymbol{v}(\boldsymbol{y}) \tag{2}$$

where $\boldsymbol{y}$ is some point in the fluid domain, and $\boldsymbol{s}(\boldsymbol{y})$ is the external force/unit volume on the fluid at $\boldsymbol{y}$. In the present work, local net charge densities, $\rho(\boldsymbol{y})$, interacting with local electric fields ($-\boldsymbol{\nabla}\Lambda(\boldsymbol{y})$ where $\Lambda(\boldsymbol{y})$ is the local electrodynamic potential) gave $\boldsymbol{s}(\boldsymbol{y}) = -\rho(\boldsymbol{y})\boldsymbol{\nabla}\Lambda(\boldsymbol{y})$. Typical in modeling, the particle is translated with velocity $\boldsymbol{u}_{\mathrm{o}}$ and rotated with angular velocity $\boldsymbol{\omega}$ about some fixed but arbitrary point, $\mathbf{o}$, located within the particle and this point is chosen as the origin of a body-fixed reference frame. At point $\boldsymbol{y}_{\mathrm{s}}$ on the particle surface, we also know the fluid velocity from the 'stick' boundary condition.

$$\boldsymbol{v}(\boldsymbol{y}_{\mathrm{s}}) = \boldsymbol{u}_{o} + \boldsymbol{\omega}x\boldsymbol{y}_{\mathrm{s}} \tag{3}$$

The fluid velocity at any point in the fluid or on S_{hyd}, subject to the stick boundary condition, is given by the following integral representation [24]

$$\boldsymbol{v}(\boldsymbol{y}) = \boldsymbol{v}_{\infty}(\boldsymbol{y}) + \boldsymbol{v}^{(0)}(\boldsymbol{y}) + \boldsymbol{v}^{(1)}(\boldsymbol{y}) \tag{4}$$

where $\boldsymbol{v}_{\infty}(\boldsymbol{y})$ is the velocity the fluid would have at $\boldsymbol{y}$ if the particle were not there,

$$\boldsymbol{v}^{(0)}(\boldsymbol{y}) = \int_{V}\boldsymbol{U}(\boldsymbol{x},\boldsymbol{y})\cdot\boldsymbol{s}(\boldsymbol{x})\mathrm{d}V_{x} \tag{5}$$

$$\boldsymbol{v}^{(1)}(\boldsymbol{y}) = -\int_{S_{\mathrm{hyd}}}\boldsymbol{U}(\boldsymbol{x},\boldsymbol{y})\cdot\boldsymbol{f}(\boldsymbol{x})\mathrm{d}S_{x} \tag{6}$$

$$U(x,y) = -\frac{1}{8\pi\eta r}\left[\boldsymbol{I} + \frac{\boldsymbol{rr}}{r^2}\right] \tag{7}$$

$$\boldsymbol{r} = \boldsymbol{y} - \boldsymbol{x}; \quad r = |\boldsymbol{r}| \tag{8}$$

$\boldsymbol{f}$ in Eq. (6) represents the hydrodynamic stress force per unit area at point $\boldsymbol{x}$ on the hydrodynamic surface of shear and can be determined from the assumed motion of the particle and boundary conditions as discussed shortly. $\boldsymbol{U}$ in Eq. (8) is a tensor representing the 'singular' solution, $\boldsymbol{I}$ is the 3×3 identity tensor, and $\boldsymbol{rr}$ the position dyadic. Also, V in Eq. (5) denotes the entire fluid volume exterior to the particle. In the

absence of external forces, which would be the case if our particle were uncharged, Eq. (5) vanishes. It is convenient to divide S_{hyd} into a series of N platelets and, if $\boldsymbol{v}^{(0)}$ is non-vanishing, the volume around the particle into M shells consisting of a total of $N^*(M-1)$ volume elements [38,39]. Since the variation in s is greatest near the particle, the thickness of the shells are chosen to increase as one moves away from the surface. An example of the partitioning of S_{hyd} for a 20-bp DNA fragment into 352 triangular platelets is shown in Fig. 1. Also illustrated by the wireframe triangles are shell numbers 5–9 corresponding to a single platelet. The assumption is made that field quantities are constant over a particular platelet (such as $\boldsymbol{v}$ or $\boldsymbol{f}$) or volume element (such as $\boldsymbol{v}$ or $\boldsymbol{s}$) but that these field quantities can vary from one platelet or volume element to the next. For point $\boldsymbol{y}_i$ at the centroid of platelet i on S_{hyd},

$$\boldsymbol{v}_i = \boldsymbol{v}_{\infty,i} + \boldsymbol{v}_i^{(0)} + \sum_{j=1}^{N} \boldsymbol{G}_{i,j} \cdot \boldsymbol{f}_j \tag{9}$$

where

$$\boldsymbol{v}_i^{(0)} = -\int_V \boldsymbol{U}(\boldsymbol{x}, \boldsymbol{y}_i) \cdot \boldsymbol{s}(\boldsymbol{x}) \mathrm{d}V_x \tag{10}$$

$$G_{i,j} = -\int_{S_j} \boldsymbol{U}(\boldsymbol{x}, \boldsymbol{y}_i) \mathrm{d}S_x \tag{11}$$

and S_j denotes the surface of platelet j. The unknowns in Eq. (9) are the $\boldsymbol{f}_j$ values since the fluid velocity in the absence of the particle, the velocity of the particle itself, and (if present) $\boldsymbol{s}(\boldsymbol{x})$ are known, or in the case of $\boldsymbol{s}(\boldsymbol{x})$, at least approximated. Eq. (9) represents $3N$ equations in $3N$ unknowns. It is convenient to write this in matrix notation as

$$\boldsymbol{v} = \boldsymbol{v}_\infty + \boldsymbol{v}^{(0)} + \boldsymbol{G} \cdot \boldsymbol{f} \tag{12}$$

where the lower case symbols represent $3N \times 1$ column vectors and the upper case $\boldsymbol{G}$ represents the $3N$ by $3N$ supermatrix made up of the N^2 3×3 $\boldsymbol{G}_{ij}$ matrices. Although large, it is straightforward to compute the $\boldsymbol{G}$ matrix once the shear

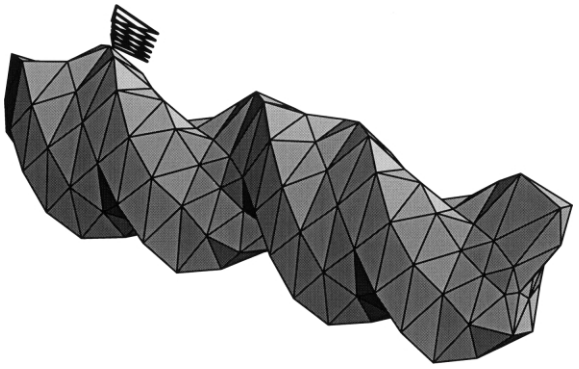

Fig. 1. Solvent accessible surface of 20-bp DNA ($pd(A)_{20} \cdot pd(T)_{20}$) represented as 352 flat triangular plates. Space exterior to the polyion in the fluid domain is subdivided into shells and each shell, in turn, is subdivided into a large number of volume elements. A few of these volume elements are illustrated by the wireframe triangles.

surface and its subdivision are defined. It can then be inverted to give

$$\mathbf{f} = \boldsymbol{G}^{-1}(\boldsymbol{v} - \boldsymbol{v}_\infty - \boldsymbol{v}^{(0)}) \tag{13}$$

Once Eq. (13) has been solved, it is straightforward to compute friction tensors as shall be discussed next. It is also straightforward to determine $\boldsymbol{v}$ throughout the fluid domain by numerically solving Eq. (4) using discretization procedures similar to that employed to determine $\boldsymbol{f}$.

Before computing various resistance tensors, it is necessary to compute total forces, $\boldsymbol{z}$, and torques, t_o, on the fluid from the relations

$$\boldsymbol{z} = \sum_i \boldsymbol{f}_i A_i + \sum_k \boldsymbol{s}_k V_k \tag{14}$$

$$\boldsymbol{t}_o = \sum_i (\boldsymbol{y}_i \boldsymbol{x} \boldsymbol{f}_i) A_i + \sum_k (\boldsymbol{y}_k \boldsymbol{x} \boldsymbol{s}_k) V_k \tag{15}$$

where 'x' denotes cross-product, the sum over i is over all surface platelets, and the sum over k is over all volume elements. The subscript 'o' appearing in Eqs. (3) and (15) and some of the tensor quantities that follow signifies that the quantity depends on the choice of origin. In a 'case 1' transport problem, the particle is trans-

lated/rotated in a fluid which is at rest except for the perturbation produced by the motion of the particle itself and its associated ion atmosphere. The total force and total torque exerted by the particle on the surrounding fluid are related to $\boldsymbol{u}_o$ and $\boldsymbol{\omega}$ by [55]

$$\boldsymbol{z}^{(1)} = \boldsymbol{\Xi}_t \cdot \boldsymbol{u}_o + \boldsymbol{\Xi}_{o,c}^T \cdot \boldsymbol{\omega} \tag{16}$$

$$\boldsymbol{t}_o^{(1)} = \boldsymbol{\Xi}_{o,c} \cdot \boldsymbol{u}_o + \boldsymbol{\Xi}_{o,r}^T \cdot \boldsymbol{\omega} \tag{17}$$

where $\boldsymbol{\Xi}_t$, $\boldsymbol{\Xi}_{o,r}$, and $\boldsymbol{\Xi}_{o,c}$ are the translation, rotation, and translation–rotation coupling resistance tensors, and the 'T' superscript denotes transpose. Also, the '(1)' superscript denotes a case 1 transport problem. By translating (but not rotating) along three orthogonal directions, and then rotating (but not translating) about three orthogonal directions, it is straightforward to compute the three tensors $\boldsymbol{\Xi}_t$, $\boldsymbol{\Xi}_{o,r}$, and $\boldsymbol{\Xi}_{o,c}$. The connections between these resistance tensors and the corresponding mobility or diffusion tensors are well known [22,55–57]. The origin dependent translational diffusion tensor, $\boldsymbol{D}_{o,t}$, and origin independent rotational diffusion tensor, $\boldsymbol{D}_r$ are given by [55,57]

$$\boldsymbol{D}_{o,t} = k_B T (\boldsymbol{\Xi}_t - \boldsymbol{\Xi}_{o,c}^T \cdot \boldsymbol{\Xi}_{o,r}^{-1} \cdot \boldsymbol{\Xi}_{o,c})^{-1} \tag{18}$$

$$\boldsymbol{D}_r = k_B T (\boldsymbol{\Xi}_{o,r} - \boldsymbol{\Xi}_{o,c} \cdot \boldsymbol{\Xi}_t^{-1} \cdot \boldsymbol{\Xi}_{o,c}^T)^{-1} \tag{19}$$

Within a numerical constant, $\boldsymbol{D}_{o,t}$ also equals the mobility tensor, $\boldsymbol{a}$, of Kim and Karilla [22]. The second terms on the right hand side of Eqs. (18) and (19) are zero in the event of no coupling of translational and rotational motions. One point of interest in what follows will be the significance of translation–rotation coupling for the detailed DNA models used in this work. Given the 'propeller-like' nature of detailed DNA models such as that illustrated in Fig. 1, we do *not* expect translation–rotation coupling to vanish. A detailed discussion of the symmetry properties of structures that exhibit translation–rotation coupling can be found elsewhere [56]. It will prove convenient to also define the following scalar quantities

$$D_t^{nc} = \frac{k_B T}{3} \mathrm{Tr}(\boldsymbol{\Xi}_t^{-1}) \tag{20}$$

$$D_t^{o} = \frac{1}{3} \mathrm{Tr}(\boldsymbol{D}_{o,t}) \tag{21}$$

where 'Tr' denotes summation over the diagonal terms of the tensor. As discussed by Garcia de la Torre and coworkers [55,57], the translational diffusion tensor is only meaningful when referred to a specific point, the center of diffusion, $\boldsymbol{d}$. They go on and give specific equations for determining $\boldsymbol{d}$ as well as the translational diffusion tensor in a reference frame with $\boldsymbol{d}$ chosen as the origin, $\boldsymbol{D}_{d,t}$. These equations will not be reproduced here. The origin independent translational diffusion constant, D_t, measured in an experiment such as light scattering [2,3] is

$$D_t = \frac{1}{3} \mathrm{Tr}(\boldsymbol{D}_{d,t}) \tag{22}$$

For the models considered in this work, the starting origin is chosen as the center of mass of the particle. The rotational diffusion tensor, translational diffusion constants D_t^{nc}, D_t^{o}, and D_t as well as $\boldsymbol{d}$ are computed as described above.

3. Diffusion constants of some (uncharged) model DNA structures

The experimentally measured translational and rotational diffusion constants of short DNA fragments can be accurately reproduced by modeling them as uncharged right circular cylinders of length L (in Å) $= 3.4 n_{bp}$ and radius $R = 10$ Å, where n_{bp} is the number of base pairs [4,6]. For this model, D_t is given by [58]

$$D_t = \frac{k_B T}{3\pi\eta L} (\ln b + \gamma) \tag{23}$$

$$\gamma = 0.312 + 0.565/b + 0.10/b^2 \tag{24}$$

where $b = L/2R$. For a 20-bp DNA in water at 20°C and $\eta = 0.01$ poise, Eqs. (23) and (24) give $D_t = 10.80 \times 10^{-7}$ cm^2/s. The experimental D_t is 10.86×10^{-7} cm^2/s in water at 20°C containing 0.10 M NaCl and 0.05 M phosphate buffer at pH 7.0 [4]. Under these relatively high salt conditions, electrolyte friction effects should be small as discussed later. We consider now the diffusion constants calculated from BE modeling that accounts for the detailed surface topography of the fragments. An all atom representation of a standard B-form 20 bp DNA fragment, or more precisely $pd(A)_{20} \cdot pd(T)_{20}$, is generated by SYBYL. The procedure used to generate the solvent accessible surface, S_{sas}, is described in detail elsewhere [39]. Basically, one rolls a 1.4-Å probe sphere over a space filling, 352 platelet model of the structure and the result is the solid object in Fig. 1. BE modeling of this uncharged model yields D_t^{nc}, D_t^o, and $D_t = 10.88 \times 10^{-7}$ cm^2/s to within 0.1% of each other. This result illustrates two important points. First of all, the fact that BE modeling of a detailed structure yields a D_t that is only 0.7% higher than the prediction of Eqs. (23) and (24) shows that the surface of hydrodynamic shear, S_{hyd}, and S_{sas}, are nearly coincident. This is consistent with earlier work [10]. The second point is that translation–rotation coupling must be negligible for this model given the near equality of D_t^{nc}, D_t^o, and D_t. As a consequence, the dependence of the various friction and diffusion/mobility tensors on the choice of origin should also be weak or negligible.

The BE method is not restricted to relatively small biomolecules such as the 20-bp DNA fragment considered above. To illustrate this, we have modeled a torsionally stressed supercoiled 375-bp closed circular DNA with a linking number of −4. Brownian dynamics simulation is first used to model the DNA as a circular string of 40 beads that are flexurally and torsionally deformable [59]. It is assumed that there are no permanent bends in the structure and a bending force constant is chosen to produce an overall persistence length of 500 Å [60]. Also, the torsional rigidity is set to 2.0×10^{-19} erg cm which lies well within the experimental range [61]. At the beginning of a dynamical trajectory, the structure is placed in a closed circular conformation that is torsionally stressed to yield a linking number of −4 [62]. The linking number, Lk, is a topological constant that equals the sum of the twist, Tw, and writhe, Wr [62]. Although Lk is constant, Tw and Wr vary with time, but for the particular structure considered here, the Tw reaches a steady state value after approximately 1 μs. It is allowed to relax for several microseconds at 20°C in water ($\eta = 0.01$ poise) to yield a representative equilibrium conformation. Since the pioneering work of Hagerman and Zimm [63], the overall transport of flexible structures have frequently been estimated by generating representative conformations, computing the transport properties of those rigid conformations, and averaging them. In the present work, we shall simply consider one representative conformation. The resultant structure generated by Brownian dynamics is sheathed in a closed circular cable consisting of 640 platelets with radius 10 Å (contour length = 1275 Å) and this is shown in Fig. 2. At 20°C in water ($\eta = 0.01$ poise), D_t^{nc}, D_t°, and $D_t = 2.187$, 2.194, and 2.197×10^{-7} cm^2/s and the center of diffusion is calculated to be at a distance of 9.4 Å from the 'center of mass'. As before, translation–rotation coupling is seen to be very small. The eigen-values of $\boldsymbol{D}_{d,t}$ are 2.581, 2.076, and 1.934×10^{-7} cm^2/s, respectively, and are 5.624, 0.529 and 0.480×10^5 1/s for $\boldsymbol{D}_r$.

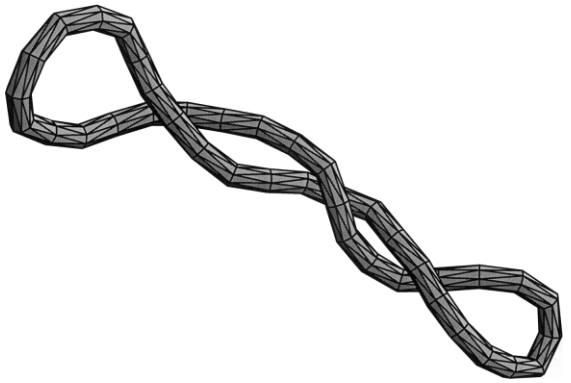

Fig. 2. BE model of a 375-bp closed circular DNA with linking number = −4. The structure, represented by 640 interconnected platelets, is flexurally and torsionally flexible.

3.1. Electrolyte friction

As pointed out in Section 1, sedimentation and diffusion constants of highly charged biomolecules are reduced because of the additional frictional drag, or electrolyte friction, that arises as a consequence of ion relaxation [40–46]. To include this effect, it is necessary determine the steady state, but non-equilibrium ion distributions near an isolated macroion in case 1 transport. The procedure employed to do this is described in detail elsewhere [37–39] so the treatment here shall be limited to an outline.

The continuum hydrodynamic–electrodynamic model employed is the continuum primitive model [64,65]. It is necessary to include in the Navier–Stokes equation [Eq. (1)] the external force/volume in the fluid domain, $\boldsymbol{s}(\boldsymbol{x})$, at point $\boldsymbol{x}$, which, in turn, requires knowledge of the electrodynamic potential, $\Lambda(\boldsymbol{x})$, and the local charge density, $\rho(\boldsymbol{x})$. The local charge density corresponds to the fixed charge density of the macroion if $\boldsymbol{x}$ lies inside the macroion and to the charge density of the mobile ion atmosphere if $\boldsymbol{x}$ lies outside. The mobile ion atmosphere is treated as a continuum. To determine $\Lambda(\boldsymbol{x})$, space is divided into a region of low dielectric constant ε_i, characteristic of the polyion interior, and a high dielectric region ε_o, characteristic of the bulk fluid. Let the surface S_d denote the boundary separating the low and high dielectric regions. In general, $\Lambda(\boldsymbol{x})$, is related to $\rho(\boldsymbol{x})$ by Poisson's equation [11,28,64,65]

$$\nabla(\varepsilon(\boldsymbol{x})\nabla\Lambda(\boldsymbol{x})) = -4\pi\rho(\boldsymbol{x}) \tag{25}$$

both inside and outside of S_d. On S_d, the normal derivative of Λ is discontinuous, but satisfies the boundary condition

$$\varepsilon_i(\nabla\Lambda(\boldsymbol{x}_s)\cdot\boldsymbol{n})_{\text{interior}} = \varepsilon_o(\nabla\Lambda(\boldsymbol{x}_s)\cdot\boldsymbol{n})_{\text{exterior}} \tag{26}$$

where $\boldsymbol{x}_s$ is a point on S_d, $\boldsymbol{n}$ is a local outward unit normal to S_d (into the domain characterized by dielectric constant ε_o) at $\boldsymbol{x}_s$, and the 'interior' ('exterior') subscripts indicate the derivative is evaluated interior (exterior) to S_d. In the present work, we set $\varepsilon_i = 4$ [66] and the exterior dielectric constant ε_o, to the value appropriate for water (80.36 and 78.3 at 20 and 25°C, respectively) [67]. Past studies of electrophoretic mobilities carried out by several different investigators with ion relaxation included have shown that they are insensitive to the choice of ε_i [32,33,68]. Because of this, it shall be assumed that S_d is coincident with S_{sas} which, in turn, is coincident with S_{hyd}. This assumption greatly simplifies the problem since the same surface used in the BE solution of the Navier–Stokes equation can be used here.

At equilibrium, the local ion density, $\rho_{eq}(\boldsymbol{x})$, is related to the equilibrium electrostatic potential, $\Lambda_{eq}(\boldsymbol{x})$, by a Boltzmann relation,

$$\begin{aligned}\rho_{eq}(\boldsymbol{x}) &= q\sum_\alpha z_\alpha n_{\alpha,eq}(\boldsymbol{x}) \\ &= q\sum_\alpha z_\alpha c_{\alpha 0} e^{-qz_\alpha\Lambda_{eq}(\boldsymbol{x})/k_BT}\end{aligned} \tag{27}$$

where the sum over α is over all mobile ion species of valence z_α, q is the protonic charge, $n_{\alpha,eq}$ is the local equilibrium concentration of species α, $c_{\alpha 0}$ is the concentration of that ion far from the macroion, T is the absolute temperature, and k_B is Boltzmann's constant. In this case, Eq. (27) reduces to the non-linear Poisson–Boltzmann equation which can be solved by an iterative BE procedure [69]. In the presence of an external flow (or electric) field, however, $\rho(\boldsymbol{x})$ will deviate, perhaps slightly, from $\rho_{eq}(\boldsymbol{x})$, and this deviation will depend on the perturbing flow (or electric) field and the mobilities of the small ions. Under these conditions, it is necessary to also solve a steady state ion transport equation for each of the mobile species present,

$$\nabla\cdot\boldsymbol{j}_\alpha = 0 \tag{28}$$

$$\boldsymbol{j}_\alpha = n_\alpha\boldsymbol{v} - D_\alpha\nabla n_\alpha + \frac{n_\alpha D_\alpha \boldsymbol{s}_\alpha}{k_BT} \tag{29}$$

where $\boldsymbol{j}_\alpha$ is the local current density of species, n_α the local concentration of that species, $\boldsymbol{v}$ the fluid velocity, D_α the diffusion constant of an α ion, and $\boldsymbol{s}_\alpha$ the local external force on an α ion. The difficulty with solving Eqs. (1), (2), (25), (28)

and (29) is that they are coupled together. For example, in order to solve Eqs. (28) and (29) for the local ion densities, n_α, we need to know $\boldsymbol{v}$ and $\boldsymbol{s}_\alpha$, but these, in turn, depend on the local ion densities. This difficulty, however, can be dealt with in an iterative cycle where successive estimates of the interrelated quantities are used to update others. To begin the cycle, we start by initially ignoring ion relaxation. In other words, ρ is approximated with ρ_{eq} [Eq. (27)] in the solution of Eq. (25) in order to obtain initial estimates of Λ and n_α throughout the fluid domain. Also Eqs. (1) and (2) are solved to obtain initial estimates of $\boldsymbol{v}$. These are then used in Eqs. (28) and (29) to obtain updated estimates of n_α. This whole cycle is repeated until all quantities converge [37]. At first glance, it might appear that charge effects would influence the diffusion of macroions even in the absence of ion relaxation since equilibrium charge densities and local electric fields produce non-vanishing local equilibrium forces, $\boldsymbol{s}_{eq}$, on the fluid. However, the net force on an *equilibrium* polyion in the absence of a perturbing flow field must vanish and hence $\boldsymbol{s}_{eq}$ makes no *net* contribution to $\boldsymbol{z}^{(1)}$ and $\boldsymbol{t}_o^{(1)}$ in Eqs. (14) and (15). In the absence of ion relaxation, charge effects can be ignored in case 1 transport and hence diffusion. When ion relaxation is accounted for, however, polyion charge does contribute to diffusion.

In order to include ion relaxation, the diffusion constants of the mobile ions, D_α, are needed, or equivalently, the mobile ion hydrodynamic radii, $r_\alpha = k_B T/6\pi\eta D_\alpha$. These are estimated from limiting molar ionic conductivities, λ_α^∞, and the Nernst–Einstein relation [70]. In an aqueous media at 25°C ($\eta = 0.89$ cp) and λ_α^∞ in 10^{-4} m^2/ohm mole, then r_α (in Å) equals $92.01 z_\alpha^2/\lambda_\alpha^\infty$. The λ_α^∞ values (in 10^{-4} m^2/ohm mol at 25°C) of K^+, Cl^-, and acetate$^-$ ($CH_3CO_2^-$ or simply Ac^-) are 73.48, 76.31 and 40.9, respectively [67]. An additional cation of interest in this work is Tris$^+$ ($(CH_2OH)_3CNH_3^+$) which has a λ_α^∞ of 29.72 [71]. In addition to the 20-base pair DNA fragment considered previously ($pd(A)_{20}\cdot pd(T)_{20}$), we shall be interested in an 18-bp fragment (5′-ACGATCACCTTTGCTCAC-3′) that has been studied by capillary electrophoresis [72]. Detailed models derived from the secondary structure are constructed for both the 18- and 20-bp fragments following the same procedure discussed in the previous section. In addition, a 60-bp fragment modeled as a 'capped cylinder', or CC, consisting of 240 platelets, is also examined. The CC models [38] do not account for the detailed surface topography of the DNA fragment, but are designed to reproduce the D_t expected using Eqs. (23) and (24). The lower object in Fig. 3 is an example of a CC model for 20-bp DNA consisting of 96 platelets. The translational diffusion constants in the absence, $D_t(nr)$, and presence, $D_t(r)$, of ion relaxation are shown in Table 1 under a number of conditions. In Tris acetate salt at pH 8.0 half of the Tris is protonated and the actual concentration of Tris$^+$ and Ac^- ions is only half the total salt concentration [27]. (Some care must be taken in identifying the actual ion concentrations in Tris buffers since they depend on how the buffers are prepared in the first place. A common practice is to start with Tris base and then add enough acid to protonate half of the Tris (N. Stellwagen, personal correspondence). It is assumed in the present work that this procedure is followed.) The salt concentrations listed in the table reflect the ion concentrations, which are simply half the total salt concentration of Tris acetate. Also note that in all but one of the Tris acetate cases, the phosphate charges in the DNA model are reduced from -1.0, which they actually should be, to -0.5. The reason for this is an assumed phosphate charge of -0.5 gives electrophoretic mobilities in better agreement with experiment when the buffer salt is Tris acetate. This point shall be discussed in more detail in the next section. From the first three entries, it is seen that reducing the salt concentration, or raising the absolute charge on the polyion, produces a greater electrolyte friction effect: $\Delta = 100(D_t(nr) - D_t(r))/D_t(nr)$. Comparing the first and last entries, it is seen that increasing the length of the DNA, and hence the total polyion charge, is predicted to have little effect on Δ. It is possible to understand this by appealing to the theory of spherical polyions [40,51]. For spheres with a central charge, it is predicted that the electrolyte friction effect is a function of the electrostatic potential averaged over the polyion surface and modeling of the

present structures predicts that these are almost equal for 18- and 60-bp DNA despite their differences in total charge. At .11 M KCl, the effect is quite small and would be difficult to measure experimentally. In addition, conditions which produce a large electrolyte friction effect (low salt and high polyion charge) also enhance interparticle interactions [51] and it becomes difficult to disentangle effects on transport due to electrolyte friction and macroion concentration. This helps explain why very little experimental work has been carried out that addresses this issue and what little there is available is inconclusive [44,51]. Since the net charge of proteins is typically much smaller than that of the DNA fragments considered here, the electrolyte friction effect is expected to be small. A transport property which is far more sensitive to the charge of a biomolecule is the electrophoretic mobility discussed next.

3.2. Free solution steady state electrophoretic mobility

In free solution steady state electrophoresis, a macroion is placed in a constant external electric field, $\boldsymbol{e}$, in a Newtonian fluid which is at rest far from the macroion. At steady state, the particle translates with uniform average velocity, $\boldsymbol{v}$, in the same or opposite direction of $\boldsymbol{e}$. In order to calculate the electrophoretic mobility, $\mu = v/|e|$ (where units on μ are typically in $cm^2/V\ s$), it is necessary to carry out additional model transport calculations, called case 2, in which the polyion is held stationary in a constant external electric field. The case 2 force, $z^{(2)}$, for the structure in a particular orientation can be written

$$z^{(2)} = -\boldsymbol{Q}\cdot\boldsymbol{e} \tag{30}$$

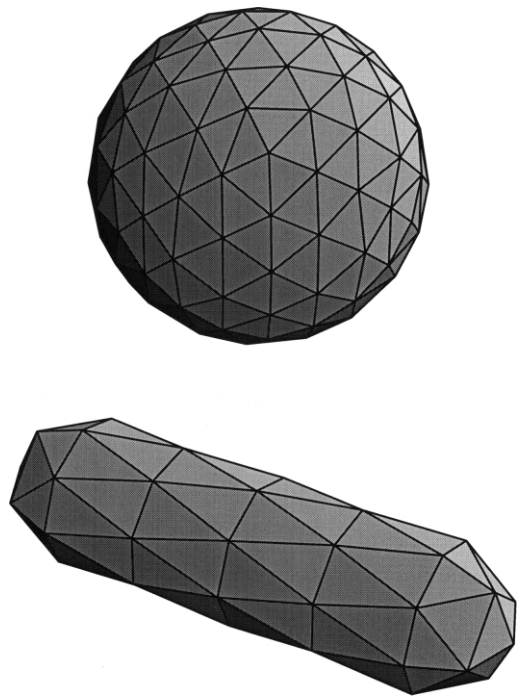

Fig. 3. Two additional BE model surfaces. The upper figure is a 20 Å radius sphere modeled by 256 platelets, and the lower figure is a 'capped cylinder', CC, model of 20-bp DNA (96 platelets).

where $\boldsymbol{Q}$ is the 'effective charge tensor'. If the counterion atmosphere can be ignored (valid for weakly charged polyions in the limit of low salt), the total force on a stationary charged particle is simply the total charge, Q_{tot}, times $\boldsymbol{e}$ so $\boldsymbol{Q} \to Q_{tot}\boldsymbol{I}$ in this limiting case. The presence of an ion atmosphere will alter this and in the general case, the total force may not necessarily be in the same direction as $\boldsymbol{e}$. Hence the identification of an

Table 1
Predicted electrolyte friction effect of DNA fragments

n_{bp}	Phosphate charge	Salt	$D_t(nr)^a$	$D_t(r)^a$	Δ
18	0.5	0.02 M $Tris^+Ac^-$	11.42	10.69	6.4
18	0.5	0.04 M $Tris^+Ac^-$	11.42	10.87	4.8
18	1.0	0.02 M $Tris^+Ac^-$	11.42	10.07	11.8
20	1.0	0.11 M KCl	10.88	10.61	2.5
60	0.5	0.02 M $Tris^+Ac^-$	5.66	5.29	6.5

[a] In 10^{-7} cm^2/s at 20°C, $\eta = 1.0$ cp.

effective charge *tensor*. All components of $\boldsymbol{Q}$ can be determined by BE calculations analogous to that employed in case 1 transport discussed previously to compute the various components of the friction tensors. From the total forces computed for e oriented along three orthogonal directions, all components of $\boldsymbol{Q}$ can be deduced. Provided the external field is small, steady state electrophoresis can be viewed as a linear superposition of case 1 and case 2 transport in which the total force on the particle vanishes. The total force on the particle is obtained by adding Eqs. (16) and (30) and setting this sum to zero. We also saw previously that the translation–rotation coupling contribution to Eq. (16) is very small in all the examples considered in this work and can be ignored to a good approximation. It is then straightforward to define the mobility tensor

$$\boldsymbol{M} = \boldsymbol{\Xi}_t^{-1} \cdot \boldsymbol{Q} \tag{31}$$

where the steady state drift velocity, $\boldsymbol{u}$, of our polyion oriented in a particular direction is related to $\boldsymbol{e}$ by the relationship $\boldsymbol{u} = \boldsymbol{Me}$. The average mobility, μ, is obtained by averaging $\boldsymbol{M}$ over all possible orientations since the field induced orientation of the particle is negligible at sufficiently weak field strength. Equivalently we can write [73] $\mu = \mathrm{Tr}\{\boldsymbol{M}\}/3$ where 'Tr' denotes 'trace' of the tensor, or summation over the diagonal components of $\boldsymbol{M}$.

Wiersema and co-workers [32] carried out extensive calculations on the mobilities of spherical polyions. As a first illustration of the BE methodology applied to free solution electrophoresis, we shall consider one example which makes direct comparison with this earlier work. The sphere radius, a, is chosen to be 20 Å, $T = 25$°C, $\eta = 0.89$ cp, and a monovalent salt concentration of 0.577 mol/l is assumed. This gives a solution with a Debye–Huckel screening parameter, [3,11,70] κ, of 0.25 Å^{-1} and $\kappa a = 5.0$. A single positive charge is placed at the center of the sphere and its magnitude chosen to give an average reduced surface potential, $y_0 = q\langle \Lambda_0 \rangle_s / k_B T$, equal to 3.00 $\pm$ 0.01. This y_0 is chosen since it is sufficiently large to insure that ion relaxation has a significant effect on μ [32]. The actual charge placed at the center of the model polyion depends slightly on the number of surface platelets, N, representing the model sphere when y_0 is held constant, but 66.5 (in protonic units) is typical. For the diffusion constants of small ions, Wiersema and co-workers chose $\lambda_\alpha^\infty = 70 \times 10^{-4}$ m^2/ohm mol for both + and − ions, which corresponds to $r_\alpha = 1.31$ Å, and that value is used in the present work. In addition, a reduced mobility, E, is defined

$$E = \frac{6\pi\eta q}{\epsilon_o k_B T}\mu \tag{32}$$

In the absence and presence of ion relaxation, E is expected to be 3.41 and 2.74, respectively [32]. The top structure shown in Fig. 3 is a sphere modeled with $N = 256$ triangular platelets. In BE modeling, the assumption is made that physical quantities such as electrostatic potential, fluid velocity, etc., are constant over a particular platelet or volume element. A straightforward way of investigating the numerical error this assumption produces is to carry out several BE calculations in which N is varied and plotting the mobility, or E vs. $1/N$. This 'extrapolated shell' procedure has been discussed previously in connection with BE modeling [24,38]. There is no fundamental reason to expect the mobility or some other transport property to vary linearly with $1/N$. In fact, a model mobility may depend on the detailed geometry of the plated structure itself and not simply on N [38]. However, the variation of mobility with N and structure geometry is fairly weak and provided accuracy to within a few percent is acceptable, a simple extrapolation of E vs. $1/N$ should be adequate. In the present work, BE modeling is carried out on three spherical structures with $N = 192$, 256 and 512. The resulting 'extrapolated shell' plot for E in the presence of ion relaxation is shown in Fig. 4. The linear least squares fit extrapolation of $1/N -> 0$ gives $E = 2.74 \pm 0.01$ which is in excellent agreement with the prediction of Wiersema and co-workers [32]. For the $N = 256$ structure shown in Fig. 3, $E = 2.85$ which is 4% higher than the extrapolated shell limit. In general, we have consistently observed that model

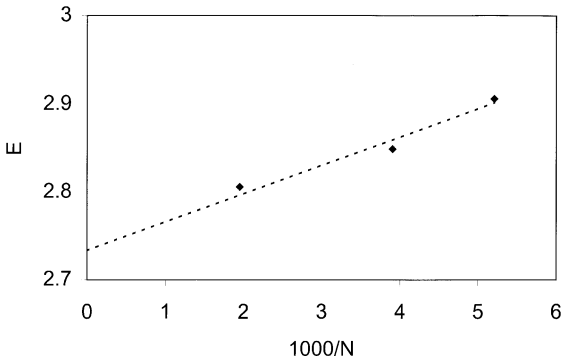

Fig. 4. Extrapolated shell plot of reduced mobility, E, for a spherical polyion. The reduced surface potential, $y_0 = 3$ and $\kappa a = 5$. Ion relaxation is included.

mobilities are slightly larger than their extrapolated shell limiting values and they need to be corrected when a high degree of accuracy is desired. Both the present BE calculations and the work of Wiersema and co-workers share the same theoretical foundations and what the study on the charged sphere example above shows is that the numerical BE algorithm is functioning correctly.

We now turn our attention to comparing calculated mobilities to actual experimental values and for that purpose, we shall consider short DNA fragments since free solution mobilities are available from several laboratories under different salt/buffer conditions [26,27]. Laue and co-workers have thoroughly studied 20 bp $pd(A)_{20}\cdot pd(T)_{20}$ at 20°C in 10 mM KCl plus 2 mM Tris–HCl at pH 8. At this pH, half of the Tris is protonated so the actual mobile ion distribution is 10 mM K^+, 1 mM $Tris^+$, and 11 mM Cl^-. Previous work has shown that it is an excellent approximation to replace the actual ion distribution above with 11 mM K^+ and Cl^- [39], and that approximation is made here. Although the $Tris^+$ counterions have a lower mobility than K^+, the fact they are present at only 10% of the concentration of K^+ makes the distinction in modeling unimportant. With regards to modeling the DNA fragments, a detailed 352-platelet model (Fig. 1) is considered as well as simpler capped cylinder models [38]. The lower object in Fig. 3 is an example of a 96 platelet capped cylinder model for 20-bp DNA designed to reproduce D_{t_o} for a right circular cylinder of axial radius 10 Å [see discussion centered around Eqs. (23) and (24)]. Also, 'extrapolated shell' capped cylinder mobilities have been estimated following the same procedure discussed above for the sphere, and this model shall be called CC for the sake of brevity. The experimental mobility measured by Laue and co-workers [26] is $-3.1 \pm 0.1 \times 10^{-4}$ cm^2/V s. Shown in Table 2 are a number of mobilities for different model cases. In the first entry, the ion atmosphere is totally ignored and we are considering the steady state transport of a polyion containing a bare charge of -40 translating at steady state in a solvent with $\eta = 1$ cp. The mobility is averaged over all possible orientations of the CC model. The absolute model mobility is over five times greater than experiment. The model employed in the second entry is identical to the first, but now the equilibrium ion atmosphere is included in the calculation of μ and μ/μ_{expt} drops from 5.51 (first entry) to 1.35. The large reduction in absolute mobility is due to the fact that the ion distribution around the polyion complements the charge of the polyion itself. When the polyion and its associated ion atmosphere are subjected to an external field, the polyion and its atmosphere will tend to move in opposite directions, and this generates a significant counter-flow of solvent near the polyion surface. This effect substantially reduces the absolute mobility and is called the 'electrophoretic effect' [32]. In the third entry, the distortion of the ion atmosphere from its equilibrium value is included and this is called the 'ion relaxation effect' [32]. Note that μ/μ_{expt} is now 1.06 which shows that at this level, modeling and experiment are in quite good agreement. The last entry is similar to the third, but now the crude CC model is replaced by a realistic surface model. In this case, $\mu/\mu_{expt} = 1.04$. What these results demonstrate is that the electrophoretic and ion relaxation effects make significant contributions to the mobility, but that the details of the polyion surface model are less important. Also, the fact that experimental and calculated mobilities are in good agreement, provided electrophoretic and ion relaxation effects are included in modeling, demon-

strates that the continuum modeling procedure employed here and in 'classical' electrophoresis theory in general [29–36], is capable of predicting free solution electrophoretic mobilities with quantitative accuracy.

Next, we consider an example quite similar to the previous 20-bp DNA case that does not give good agreement between modeling and experiment. It is an 18-bp DNA fragment (5′-ACGATCACCTTTGCTCAC-3′) studied by Stellwagen and co-workers by capillary electrophoresis [72]. The experiments were carried out at 25°C ($\eta = 0.89$ cp) in 40 mM Tris acetate at pH 8. At this pH, half of the Tris is protonated and in modeling we assume the $Tris^+$ and Ac^- ambient concentrations are 20 mM, respectively. In all of the model results reported here, the electrophoretic and relaxation effects are included in modeling and are summarized in Table 3. The first entry in the table is an extrapolated shell, capped cylinder (CC) model with 36 phosphate charges of -1 each placed on double helical spirals within the cylinder. The calculated μ is substantially larger than the experimental value, μ_{expt}, of $3.29 \pm 0.03 \times 10^{-4}$ cm^2/V s. Laue and co-workers (personal correspondence) obtain a similar experimental mobility on a 20-bp fragment employing membrane-confined analytical electrophoresis, when corrected for temperature/viscosity differences, so the discrepancy is not due to any systematic error in measurement. Thus, the same model which worked quite well in KCl does not work so well in Tris acetate. Physically, an absolute mobility measured experimentally that is lower than expected could be an indication of an interaction/association of the $Tris^+$ cations for the DNA in addition the classical electrostatic interaction. The classical electrostatic interaction is included in BE modeling, but no additional interaction such as hydrogen bonding is. In order to account for this interaction in an approximate way, we simply reduced the DNA phosphate charges of the DNA by 50% to mimic possible 'binding' of $Tris^+$ cations to the DNA. When this is done, good agreement between experimental and model mobilities is achieved. Given earlier successes in correctly predicting the electrophoretic mobilities of model spheres and DNA fragments in KCl salt, we feel confident that the mobility studies of DNA in Tris acetate are showing that there are indeed 'binding' interactions between the counterion $Tris^+$ and the DNA that are not accounted for classically. This last example shows us that electrophoretic modeling studies may, in fact, reveal structural surprises that were not anticipated beforehand.

The phenomenon of 'ion relaxation' has been one of the central themes of this work, and it is perhaps fitting that we end with a visual demonstration of it. Consider the example of an 18-bp DNA 'detailed' model (previous paragraph) translating at steady state along its helix axis in a constant external electric field, $\boldsymbol{e}$. Shown in Fig. 5 is a contour diagram of the perturbed ion density, $\delta\rho(\boldsymbol{x}) = \rho(\boldsymbol{x}) - \rho_{eq}(\boldsymbol{x})$ through a plane that contains the helix axis of the fragment. The field, $\boldsymbol{e}$, is directed downward in the figure and the motion of the particle is upward. White (black) shading corresponds to a large and positive (negative) $\delta\rho(\boldsymbol{x})$, and neutral gray shading to $\delta\rho(\boldsymbol{x}) \approx 0$. The DNA interior is represented by a neutral gray. Clearly ion relaxation is largely dipolar in character. The visualization of ion relaxation as well as other field quantities was considered previously for CC models of short DNAs [74].

Table 2
Mobilities, μ, of 20-bp DNA at 20°C (μ in 10^{-4} cm^2/V s)

Model	μ	μ/μ_{expt}
Capped cylinder, CC, no salt	17.08	5.51
CC, 11 mM KCl, no ion relaxation	4.19	1.35
CC, 11 mM KCl, ion relaxation	3.27	1.06
352 platelet detailed, 11 mM KCl, ion relaxation	3.22	1.04

Table 3
Mobilities of 18-bp DNA at 25°C in 40 mM Tris acetate (μ in 10^{-4} cm^2/V s)

Model	Charge	μ	μ/μ_{expt}
CC	−36	4.20	1.28
CC	−18	3.40	1.03
320 platelet detailed	−18	3.31	1.01

4. Summary

The primary objective of this work has been to illustrate the usefulness of boundary element modeling in biophysics by applying it to a number of specific transport problems. The most straightforward application is the prediction of diffusion constants of biomolecules modeled as uncharged, rigid arrays of triangular platelets. From 'detailed' modeling of a short DNA fragment, it was concluded that the solvent accessible and hydrodynamic shear surfaces are coincident to a good approximation. We also considered a closed-circular super-coiled DNA to show BE modeling can be applied to model biomolecules of considerable complexity. Although most biomolecules in solution are charged, it is a good approximation to ignore this in modeling sedimentation, diffusion, and intrinsic viscosities provided the ion atmosphere is not significantly distorted from its equilibrium value. As a general rule, this 'ion relaxation' effect becomes important if the magnitude of the average reduced surface potential, $y_0 = |q\langle\Lambda_0\rangle_s/k_BT|$, exceeds approximately 1 [29,32,40,48]. Although this condition is satisfied for many biomolecules (weakly charged proteins, for example), one important case where it is not satisfied is DNA [75]. Ion relaxation produces additional frictional drag on polyions which is called 'electrolyte friction'. We examined the effects of electrolyte friction on short DNA fragments and predict approximately a 2–12% reduction in D_t depending on the salt concentration and, to a lesser extent, the nature of the counterion. It should be pointed out that there are several theories of electrolyte friction [40–42,46] which arrive at different conclusions regarding the magnitude of the effect. Two short commentaries [43,44] provide a clear physical picture of the issues involved. Basically, the 'classical' approach of Overbeek [29], Booth [40], and Stigter [41] predict a substantially *smaller* electrolyte friction effect than predicted by Schurr [42] and others [46]. The present BE modeling predictions are based on the classical theory. Because the effect is evidently small and difficult to disentangle from other factors which contribute to the diffusion of highly charged polyions at low salt [45,51], there is a vital need for more experimental work to be carried out since we currently do

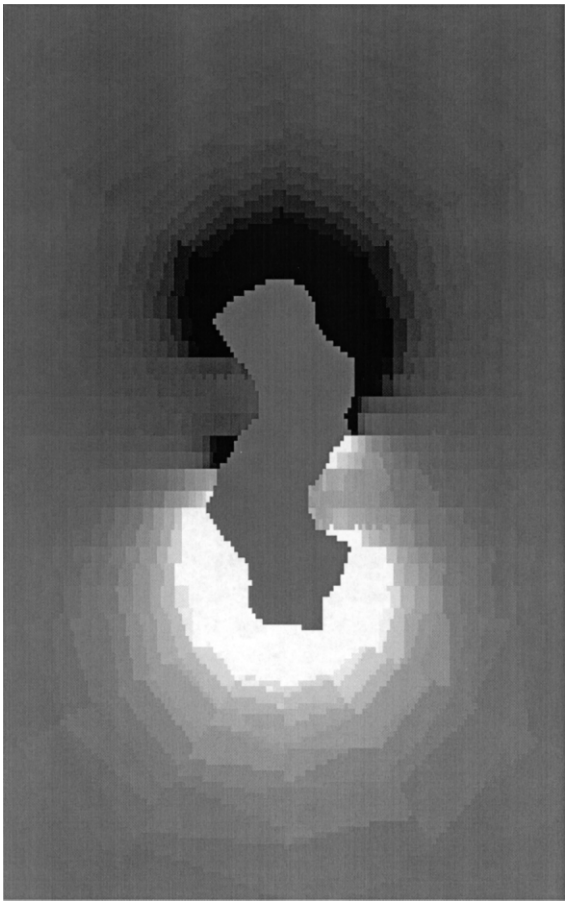

Fig. 5. Perturbed ion density, $\delta\rho(\boldsymbol{x})$, of an 18-bp DNA fragment in steady state electrophoresis translating parallel to the helix axis. A contour diagram in a plane which bisects the helix axis. The motion of the fragment would be vertically upward in the figure. White (black) shading corresponds to a large positive (negative) $\delta\rho(\boldsymbol{x})$ and a neutral gray to $\delta\rho(\boldsymbol{x}) \approx 0$. The DNA interior is shaded a neutral gray.

not even know how large the effect is in a well defined system.

The free solution electrophoretic mobility is a transport property that is particularly sensitive to charge effects and several examples were considered that made direct comparison possible between BE modeling and: (a) earlier theory on spherical polyions; (b) experiments on highly charged DNA fragments. The initial comparison showed that BE modeling is in excellent agreement with previous theory. The case of 20-bp DNA in KCl solution shows that the continuum model employed in classic electrophoresis theory is capable of yielding quantitative agreement with experiment, at least under specific solvent/buffer solutions. However, the mobility of the final example of 18-bp DNA in Tris acetate solution could not be reproduced by modeling unless the phosphate charge of the DNA is substantially reduced. Given the successes in the other examples considered, we believe what this is telling us is that there is an association between $Tris^+$ counterions and DNA that is not accounted for in modeling, perhaps hydrogen bonding.

Finally, other transport properties not considered in the present work, but which could be studied by BE modeling include intrinsic viscosity [50], electrical conductivity [76], and electric birefringence/dichroism [77–82]. At the present time, there is limited experimental data with regards to viscosity and conductivity on systems which could be realistically modeled as rigid structures. There is a considerable experimental birefringence/dichroism data on DNA fragments [77–79], but there are particularly difficulties related to theoretical modeling [81,82] which must be dealt with before the BE procedure can be applied to that problem. Work on the birefringence/dichroism problem is currently underway in this laboratory.

Acknowledgements

The author would like to acknowledge National Science Foundation grant MCB-9807541 for partial support of this work.

References

[1] H. Fujita, Foundations of Ultracentrifugal Analysis, Wiley, New York, 1975.
[2] B.J. Berne, R. Pecora, Dynamic Light Scattering by Macromolecules, Wiley, New York, 1976.
[3] K.S. Schmitz, An Introduction to Dynamic Light Scattering by Macromolecules, Academic Press, New York, 1990.
[4] W. Eimer, R. Pecora, Rotational and translational diffusion of short rodlike molecules in solution: oligonucleotides, J. Chem. Phys. 94 (1991) 2324–2329.
[5] T. Tao, Time-dependent fluorescence depolarization and Brownian rotational diffusion coefficients of macromolecules, Biopolymers 8 (1969) 609–632.
[6] S. Nuutero, B.S. Fujimoto, P.F. Flynn, B.R. Reid, N.S. Ribeiro, J.M. Schurr, The amplitude of local angular motions of purines in DNA in solution, Biopolymers 34 (1994) 463–480.
[7] S.H. Harding, The intrinsic viscosity of biological macromolecules, progress in measurement, interpretation and application to structure in dilute solution, Prog. Biophys. Mol. Biol. 68 (1998) 208–262.
[8] M.F. Sanner, A.J. Olson, T.-C. Spehner, Reduced surface: An efficient way to compute molecular surfaces, Biopolymers 38 (1996) 305–320.
[9] J.A. McCammon, S.C. Harvey, Dynamics of Proteins and Nucleic Acids, Chapter 2, Cambridge University Press, Cambridge, UK, 1987.
[10] D. Stigter, Mobility of water near charged interfaces, Adv. Colloid Interface Sci. 16 (1982) 253–265.
[11] C. Tanford, Physical Chemistry of Macromolecules, Wiley, New York, 1971.
[12] K.E. Van Holde, Physical Biochemistry, Prentice Hall, Englewood Cliffs, New Jersey, 1971.
[13] J.G. Kirkwood, J. Riseman, The intrinsic viscosity and diffusion constants of flexible macromolecules in solution, J. Chem. Phys. 16 (1948) 565–573.
[14] R.K. Dewan, K.E. Van Holde, Role of hydrodynamic interaction in the diffusion of *n*-alkanes in carbon tetrachloride, J. Chem. Phys. 39 (1963) 1820–1824.
[15] J.A. McCammon, J.M. Deutch, Frictional properties of nonspherical multisubunit structures. Application to tubules and cylinders, Biopolymers 15 (1976) 1397–1408.
[16] J. Garcia de la Torre, V.A. Bloomfield, Hydrodynamic properties of macromolecular complexes. I. Translation, Biopolymers 16 (1977) 1747–1763.
[17] D.C. Teller, E. Swanson, C. De Haen, The translational friction coefficient of proteins, Meth. Enzymol. 61 (1979) 103–124.
[18] J. Garcia de la Torre, V.A. Bloomfield, Hydrodynamic properties of complex, rigid, biological macromolecules: Theory and application, Q. Rev. Biophys. 14 (1981) 81–139.

[19] J. Garcia de la Torre, S.E. Harding, B. Carrasco, Calculation of NMR relaxation, covolume, and scattering-related properties of bead models using the SOLPRO computer program, Eur. Biophys. J. 28 (1999) 119–132.
[20] G.K. Youngren, A. Acrivos, Stokes flow past a particle of arbitrary shape: A numerical method of solution, J. Fluid Mech. 69 (1975) 377–403.
[21] G.K. Youngren, A. Acrivos, Rotational friction coefficients for ellipsoids and chemical molecules with the slip boundary condition, J. Chem. Phys. 63 (1975) 3846–3848.
[22] S. Kim, S.J. Karrila, Microhydrodynamics: Principles and Selected Applications, Butterworth-Heinemann, Boston, 1991.
[23] D. Brune, S. Kim, Predicting protein diffusion coefficients, Proc. Natl. Acad. Sci. USA 90 (1993) 3835–3839.
[24] S.A. Allison, Low Reynolds number transport properties of axisymmetric particles employing stick and slip boundary conditions, Macromolecules 32 (1999) 5304–5312.
[25] O. Vesterberg, A short history of electrophoretic methods, Electrophoresis 14 (1993) 1243–1249.
[26] T.M. Laue, T.M. Ridgeway, J.O. Wooll, H.K. Shepard et al., Insights into a new analytical electrophoresis apparatus, J. Pharm. Sci. 85 (1996) 1331–1335.
[27] N.C. Stellwagen, C. Gelfi, P.G. Righetti, The free solution mobility of DNA, Biopolymers 42 (1997) 687–703.
[28] J.D. Jackson, Classical Electrodynamics, Wiley, New York, 1975.
[29] J.T.G. Overbeek, Theorie der electrophorese. Der relaxationseffekt, Kolloid-Beih. 54 (1943) 287–364.
[30] S.A. Allison, D. Stigter, A commentary on the screened-Oseen, counterion condensation formalism of polyion electrophoresis, Biophys. Chem. 78 (2000) 121–124.
[31] F. Booth, The cataphoresis of spherical, solid, non-conducting particles in a symmetric electrolyte, Proc. R. Soc. Lond. Ser. A. 203 (1950) 514–533.
[32] P.H. Wiersema, A.L. Loeb, J.T.G. Overbeek, Calculation of the electrophoretic mobility of a spherical colloid particle, J. Colloid Interface Sci. 22 (1966) 78–99.
[33] R.W. O'Brien, L.R. White, Electrophoretic mobility of a spherical colloid particle, J. Chem. Soc. Faraday Trans. 2 (74) (1978) 1607–1626.
[34] D. Stigter, Electrophoresis of highly charged colloidal cylinders in univalent salt solutions. I. Mobility in transverse field, J. Phys. Chem. 82 (1978) 1417–1423.
[35] D. Stigter, Electrophoresis of highly charged colloidal cylinders in univalent salt solutions. 2. Random orientation in an external field and application to polyelectrolytes, J. Phys. Chem. 82 (1978) 1424–1429.
[36] Y.E. Solomentsev, Y. Pawar, J.L. Anderson, Electrophoretic mobility of nonuniformly charged spherical particles with polarization of the double layer, J Colloid Interface Sci. 158 (1993) 1–9.
[37] S.A. Allison, Modeling the electrophoresis of rigid polyions. Inclusion of ion relaxation, Macromolecules 29 (1996) 7391–7401.
[38] S.A. Allison, S. Mazur, Modeling the free solution electrophoretic mobility of short DNA fragments, Biopolymers 46 (1998) 359–373.
[39] S. Mazur, C. Chen, and S.A. Allison, Modeling the electrophoresis of short duplex DNA: Counterions K^+ and $Tris^+$, J. Phys. Chem. B (2001) (in press).
[40] F. Booth, Sedimentation potential and velocity of solid spherical particles, J. Chem. Phys. 22 (1954) 1956–1968.
[41] D. Stigter, Primary charge effect on the sedimentation of long, colloidal rods, J. Phys. Chem. 86 (1982) 3553–3558.
[42] J.M. Schurr, A theory of electrolyte friction on translating polyelectrolytes, Chem. Phys. 45 (1980) 119–132.
[43] U. Geigenmuller, Comment on electrolyte friction, Chem. Phys. Lett. 110 (1984) 666–667.
[44] J.M. Schurr, Reply to comment on electrolyte friction, Chem. Phys. Lett. 110 (1984) 668–670.
[45] S. Gorti, L. Plank, B.R. Ware, Determination of electrolyte friction from measurements of the tracer diffusion coefficients, mutual diffusion coefficients, and electrophoretic mobilities of charged spheres, J. Chem. Phys. 81 (1984) 909–914.
[46] A. Vizcarra-Rendon, M. Medina-Noyola, R. Klein, Electrolyte friction on non-spherical polyions, Chem. Phys. Lett. 173 (1990) 397–402.
[47] F. Booth, The electroviscous effect for suspensions of solid spherical particles, Proc. R. Soc. Lond. 203A (1950) 533–551.
[48] J.D. Sherwood, The primary electroviscous effect in a suspension of spheres, J. Fluid Mech. 101 (1980) 609–629.
[49] J.D. Sherwood, The primary electroviscous effect in a suspension of rods, J. Fluid Mech. 111 (1981) 347–366.
[50] S.A. Allison, The primary electroviscous effect of rigid polyions of arbitrary shape and charge distribution, Macromolecules 31 (1998) 4464–4474.
[51] K.S. Schmitz, Macroions in Solution and Colloidal Suspension, VCH Publishers, New York, 1993.
[52] O.A. Ladyzhenskaya, The Mathematical Theory of Viscous Incompressible Flow, Gordon and Breach, New York, 1963.
[53] C.-M. Hu, R. Zwanzig, Rotational friction coefficients for spheroids with the slipping boundary condition, J. Chem. Phys. 60 (1974) 4354–4357.
[54] D.R. Bauer, B.R. Alms, J.I. Brauman, R. Pecora, Depolarized Rayleigh scattering and ^{13}C NMR studies of anisotropic molecular reorientation of aromatic compounds in solution, J. Chem. Phys. 61 (1974) 2255–2261.
[55] J.M. Garcia Bernal, J. Garcia de la Torre, Transport properties and hydrodynamic center of rigid macromolecules with arbitrary shapes, Biopolymers 19 (1980) 751–766.
[56] J. Happel, H. Brenner, Low Reynolds Number Hydrodynamics, Chapter 5, Martinus Nijhoff, The Hague, 1983.
[57] J. Garcia de la Torre, A. Jimeniz, J.J. Freire, Monte Carlo calculations of hydrodynamic properties of freely

jointed, freely rotating, and real polymethylene chains, Macromolecules 15 (1982) 148–154.
[58] M.M. Tirado, J. Garcia de la Torre, Translational friction coefficients of rigid symmetric top macromolecules, J. Chem. Phys. 71 (1979) 2581–2587.
[59] S.A. Allison, J.M. Schurr, Effect of regular anisotropic permanent bending on the diffusional spinning and fluorescence polarization anisotropy of short DNA fragments studied by Brownian dynamics simulation, Macromolecules 30 (1997) 7131–7142.
[60] J.A. Schellman, S.C. Harvey, Static contributions to the persistence length of DNA and dynamic contributions to DNA curvature, Biophys. Chem. 55 (1995) 95–114.
[61] P.J. Heath, J.B. Clendenning, B.S. Fujimoto, J.M. Schurr, Effect of bending strain on the torsion elastic constant of DNA, J. Mol. Biol. 260 (1996) 718–730.
[62] G. Chirico, J. Langowski, Brownian dynamics simulation of supercoiled DNA with bent sequences, Biophys. J. 71 (1996) 955–971.
[63] P.J. Hagerman, B.H. Zimm, Monte Carlo approach to the analysis of the rotational diffusion of wormlike chains, Biopolymers 20 (1981) 1481–1502.
[64] H. Eyring, D. Henderson, B.S. Stover, E.M Eyring, Statistical Mechanics and Dynamics, Chapter 14, Wiley, New York, 1964.
[65] D.A. McQuarrie, Statistical Mechanics, Chapter 15, Harper & Row, New York, 1976.
[66] B.H. Honig, W.L. Hubbell, R.F. Flewelling, Electrostatic interactions in membranes and proteins, Ann. Rev. Biophys. Biophys. Chem. 15 (1986) 163–193.
[67] CRC Handbook of Chemistry and Physics, 74th ed., in: D.R. Linde (Ed.), CRC Press, Boca Raton, Florida, 1993.
[68] S.A. Allison, M. Potter, J.A. McCammon, Modeling the electrophoresis of lysozyme. II. Inclusion of ion relaxation, Biophys. J. 73 (1997) 133–140.
[69] H.-X. Zhou, Macromolecular electrostatic energy within the non-linear Poisson–Boltzmann equation, J. Chem. Phys. 100 (1994) 3152–3162.
[70] G.W. Castellan, Physical Chemistry, Chapter 31, 3rd ed., Addison Wesley, Reading, MA, 1983.
[71] S.D. Klein, R.G. Bates, Conductance of Tris (hydroxymethyl)-aminomethane hydrochloride (Tris–HCl) in water at 25 and 37°C, J. Sol. Chem. 9 (1980) 289–292.
[72] N.C. Stellwagen, C. Gelfi, P.G. Righetti, DNA-histidine complex formation in isoelectric histidine buffers, J. Chromatogr. A 838 (1999) 179–189.
[73] G. Arfken, Mathematical Methods for Physicists, Chapter 3, 2nd ed., Academic Press, New York, 1970.
[74] S.A. Allison, H. Wang, T.M. Laue, T.J. Wilson, J.O. Wooll, Visualizing ion relaxation in the transport of short DNA fragments, Biophys. J. 76 (1999) 2481–2501.
[75] J.A. Schellman, D. Stigter, Electrical double layer, zeta potential, and electrophoretic charge of double-stranded DNA, Biopolymers 16 (1977) 1415–1434.
[76] D. Stigter, Theory of conductance of colloidal electrolytes in univalent salt solutions, J. Phys. Chem. 83 (1979) 1670–1683.
[77] N.C. Stellwagen, Electric birefringence of restriction enzyme fragments of DNA: Optical factor and electric polarizability as a function of molecular weight, Biopolymers 20 (1981) 399–434.
[78] J.G. Elias, D. Eden, Transient electric birefringence study of the persistence length and electrical polarizability of restriction fragments of DNA, Macromolecules 14 (1981) 410–419.
[79] P.J. Hagerman, Investigation of the flexibility of DNA using transient electric birefringence, Biopolymers 20 (1981) 1503–1535.
[80] S. Diekmann, W. Hillen, B. Morgeneyer, R.D. Wells, D. Porschke, Orientation relaxation of DNA restriction fragments and the internal mobility of the double helix, Biophys. Chem. 15 (1982) 263–270.
[81] M. Fixman, Charged macromolecules in external fields. 2. Preliminary remarks on the cylinder, Macromolecules 13 (1980) 711–716.
[82] M. Fixman, S. Jagannathan, Electrical and convective polarization of the cylindrical macroions, J. Chem. Phys. 75 (1981) 4048–4059.